Delft University of Technology

Bachelor Thesis

Applied Physics

Optimizing Viscometer for Ultrasonic Nondestructive Testing with Finite Element Software

by

Anne Maaike Gerritsma

to obtain the degree of Bachelor of Science
to be defended publicly on January 15th, 2019 at 14:30

Project duration:
September 10th 2018 - January 15th 2019
Thesis committee:
MSc. S. Mastromarino,
Dr. ir. M. Rohde,
Prof. dr. ir. J. L. Kloosterman,

December 21, 2018

TU Delft Delft University of Technology

Abstract

In this thesis, a nondestructive method for measuring viscosity of a low viscous fluid, with shear horizontal waves, is evaluated. This method is mainly used in high temperature, highly corrosive and radioactive environments. The setup of this method consists of a metal waveguide partially immersed in a fluid. Using a piezoelectric transducer, a non-dispersive shear horizontal wave is excited at the top of the waveguide.

The main goal in this thesis, is to optimize the setup of this nondestructive viscometer with a finite element software. The wave behavior, in an immersed waveguide, can be described with an acoustic model. For an accurate acoustic model, the step size of the solver is optimized. Moreover, to find a balance between computation time and accuracy, the size of the waveguide is minimized. The accuracy of the model is studied by comparing the velocity of the wave inside the waveguide, found by the model, to the theoretical wave velocity.

The optimal scaling factor, for the time step size of the solver, was found to be 0.08. For the plate width, the optimal width product of the tungsten plate was found to be 2 MHz $\cdot$ 10 mm. The relative error of the wave velocity, found by the model, had a value of 1.2%. It should be investigated if by decreasing the width to length ratio, i.e. increasing the length of the plate, this error becomes smaller.

For future studies, it is recommended to investigate the effects of different plate widths on the attenuation. Since the attenuation is obtained from the difference in signal strengths, between two different immersion depth, the inaccuracy, introduced by a less optimal plate width, might vanish.

Contents

Nomenclature

Roman letters

E	Modulus of elasticity	[Pa]
G	Shear modulus	[Pa]
k	Wave number	[rad m^{-1}]
k_F	Wave number for longitudinal waves in fluids	[rad m^{-1}]
k_L	Wave number for longitudinal waves in solids	[rad m^{-1}]
k_S	Wave number for shear waves in solids	[rad m^{-1}]
M	Size of the mesh elements	[m]
N	Amount of mesh elements per wavelength	[ ]
p	Pressure, the force applied per unit area	[Pa]
T	Stress tensor	[Pa]
V_0	Bulk velocity of longitudinal waves in fluids	[m s^{-1}]
V_L	Bulk velocity of longitudinal waves in solids	[m s^{-1}]
V_S	Bulk velocity of shear waves in solids	[m s^{-1}]
V_{group}	Group velocity of ultrasonic waves	[m s^{-1}]

Greek letters

α_{Long}	Attenuation coefficient for longitudinal waves	[dB m^{-1}]
α_{SH}	Attenuation coefficient for shear horizontal waves	[dB m^{-1}]
ϵ_{ij}	Strain component resulting from stress	[ ]
η	Dynamic viscosity of the immersion fluid	[Pa s]
λ	Lamé's first parameter	[Pa]
λ_{SH}	Wavelength of shear horizontal ultrasonic waves	[m]
μ	Lamé's second parameter	[Pa]
ν	Poisson's ratio	[ ]
ρ	Density of the surrounding solid	[kg m^{-3}]
ρ_0	Density of the surrounding fluid	[kg m^{-3}]
σ_{ij}	Stress component acting on a plane	[Pa]
υ	Kinematic viscosity	[m^2 s^{-1}]
χ	Compressibility	[Pa^{-1}]
ω	Angular frequency	[rad s^{-1}]

Chapter 1

Introduction

With the current trend of global warming, the need for low-carbon technologies has become more prominent. The possibilities of a nuclear power plant to provide a low-carbon base load supply of electricity, has attracted much interest in nuclear energy. However, after the nuclear disasters in Fukushima and Chernobyl, the most common type of nuclear reactor, the pressurized water reactor, has proven to be a potential radiological hazard. Contrary to the pressurized water reactor, the molten salt fast reactor has the potential to offer safe and clean nuclear energy.

To prove nuclear energy can be inherently safe, the research group SAMOFAR (Safety Assessment of the Molten Salt Fast Reactor) has been providing experimental and numerical studies for the safety concepts of the MSFR [1]. This thesis is part of the SAMOFAR research project. For the safety assessment of the MSFR, it is important to have detailed information on the physical properties of the fuel salt.

1.1 Molten Salt Fast Reactor

The concept of the molten salt reactor date back to 1960, when it was first designed by the Oak Ridge National Laboratory as a means to fuel an aircraft. The Molten Salt Fast Reactor (MSFR) is a generation IV molten salt reactor with a liquid salt operating as fuel and coolant[2]. This reactor operates at ambient pressure and temperatures of 750°C[3]. The advantage of this low operating pressure is that the risk of a leak or break is significantly reduced. Another advantage of the MSFR is the fact that harmful isotopes are bound to the salt and therefore unable to become airborne in case of a leakage.

The main components of the MSFR are: the cylindrical vessel filled with liquid salt, the bubble injection system, fertile blanket, pumps for circulation of the fuel salt, liquid gas separation and sampling systems, external heat exchangers and a emergency storage tank. In figure 1.1, the schematic representation of the main components in the fuel circuit of the MSFR can be seen.

The initial composition of the fuel molten salt, in the MSFR, consist of lithium, thorium, uranium and plutonium fluorides (LiF-ThF_4-UF_4-PuF_4). The fuel salt enters the cylindrical reactor vessel from the bottom and is extracted at the top of the vessel. Here, the fuel salt is pumped into 16 loops of external heat exchangers. In these external heat exchangers, the heat is transfered to a secondary liquid-salt coolant [2].

To improve the breeding process in the reactor vessel, fertile blankets, comprising of thorium salts, are implemented on to the core wall[4].

Since the fertile element thorium does not contain fissile isotopes, the reactor requires initial fissile materials, such as uranium and plutonium to start[3]. To remove the fission products, neutral gas

bubbles are injected into the core and later separated from the liquid. Another treatment to remove fission products is the mini-batch on-site reprocessing. This process can also adjusts the fuel's fissile isotopes to fertile isotopes ratio, if needed[3]. These two types of treatments can be applied without stopping te reactor[4].

At the bottom of the reactor vessel, a drain plug, leading to emergency storage tank, is present. This drain plug is made from frozen salt. In case of overheating or electric power failure, the frozen plug melts and the fuel salt is drained into the external sub critical storage tank. This tank is surrounded by a large water pool, which acts as a thermal buffer for the fuel salt[3].

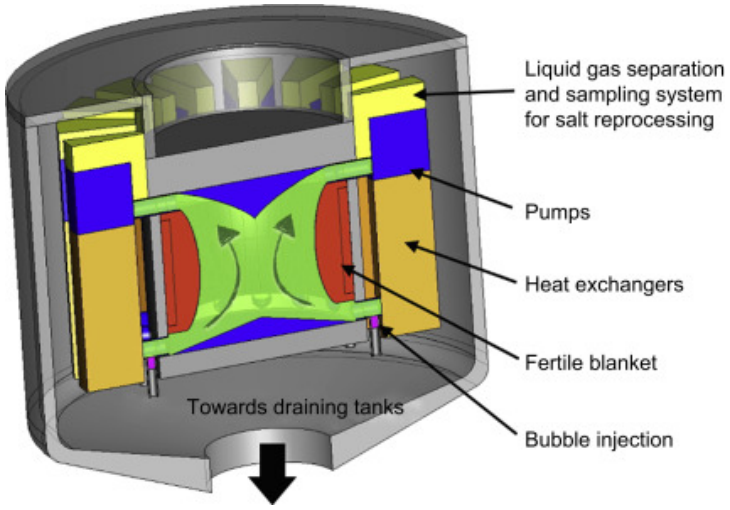

Figure 1.1: The schematic representation of the fuel circuit of the MSFR[3].

1.2 Importance of Measuring Viscosity

Since the fuel salt of the MSFR also operates as an coolant, it is important to know the efficiency of the liquid salt as heat transfer medium. To understand the heat transfer of the fuel salt, it is necessary to be able to accurately measure the viscosity. This thermodynamic property predicts the flow and the turbulent heat transfer of the fuel through the reactor circuit[5]. Viscosity, together with the density, determines the Reynolds number. This number predicts if the fluid flow will be laminar or turbulent.

Measuring the viscosity of liquid salt introduces many challenges. The first challenge is that fluoride salts are low viscous fluids at high temperature [5]. Moreover, conventional instruments are unable to withstand the corrosive, high temperature and radioactive environment of the liquid salts. Therefore, a different method for measuring the viscosity is introduced: ultrasonic non-destructive testing (NDT).

Ultrasonic NDT is a method where the thermodynamic properties of a fluid can be evaluated without causing damage to the equipment. This report focuses on the method of NDT using a waveguide and a piezoelectric transducer. Using a waveguide allows the transducer to be protected from high temperature and high corrosive environment. Moreover, using the right material for the waveguide, the waveguide will also be able to withstand the radioactive environment.

The setup, of the ultrasonic NDT method, consists of a small metal plate partially immersed in a fluid. The fluid is contained in a small vessel underneath the waveguide. By means of a piezoelectric transducer a ultrasonic wave is excited on top of the metal plate.

The setup of ultrasonic NDT method for measuring the viscosity, can be seen in the figure below.

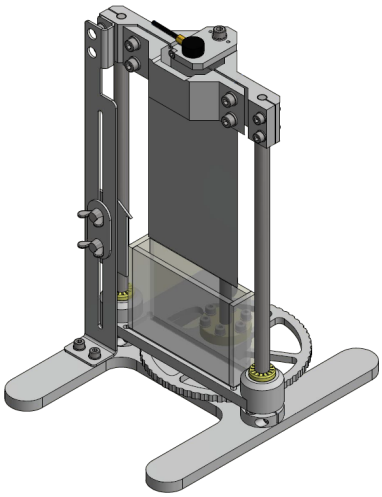

Figure 1.2: The schematic set-up of the waveguide[6].

For measuring the viscosity of a fluid, the attenuation of the transmitted wave, inside the waveguide, should be evaluated with non-dispersive waves[7]. The attenuation of a wave describes the loss or absorption of the wave energy by the medium. The attenuation measured inside the partially immersed waveguide, will contain information about the viscosity of the fluid. Since the first mode of shear horizontal ultrasonic waves is non-dispersive, these waves are preferred for this research[8].

The propagation of waves though the waveguide in this setup can be described by an acoustic model. A reliable acoustic model is an important tool for the optimization of this setup.

1.3 Goal

The goal of this research is to optimize the setup of the ultrasonic viscometer with a finite element software. Previous studies have suggested that the dimension of the plate, immersion depth and the frequency of the pulse, influence the attenuation of ultrasonic waves[8]. The aim of this research is to investigate another possible influence on this attenuation; the volume of the fluid, surrounding the partially immersed waveguide.

For this research an accurate model is needed. The accuracy of the model is mainly determined by the mesh size and the time step size of the solver. For the mesh size, the results from a previous study will be used[9]. To determine the optimal scaling factor for the time step size, the peak time for different scaling factors are evaluated.

For the model, a tungsten waveguide is used. To find a balance between accuracy of the model and computation time, the size of the plate is minimized. The accuracy of this minimized model is studied by comparing the velocity of the wave, computed by the model, to the theoretical value.

To understand the wave propagation of ultrasonic waves, the theory of elasticity is described in chapter 2. Moreover, the nondestructive method for measuring viscosity of a low viscous fluid is evaluated in this chapter. In chapter 3 the experimental method is described. Chapter 4 will state the results of the finite element software. Lastly, in chapter 5 the conclusion and recommendation are described.

Chapter 2

Theory

In this chapter the theory of elasticity is described to better understand the propagation of ultrasonic waves through a medium.

Moreover, the method for measuring the viscosity with non-destructive testing is described.

2.1 Theory of Elasticity

The theory of elasticity is part of continuum mechanics, which describes the propagation of small stresses and strains though a medium [10]. In this section, only isotropic media, such as metals, are considered. A material is isotropic when it is uniform in all directions[11].

2.1.1 Stress Tensor

Stress can be described as the force between neighboring particles per unit area $\left[\frac{N}{m^2}\right]$. There are two types of stress component, which are dependent on the orientation of the normal vector. If the force vector is normal to the surface, it is called normal stress. The other type of stress component, when the force vector is perpendicular to the surface, is called shear stress [10].
Since stress is a function of the orientation of the normal vector, a tensor is needed to describe the stress state of a solid. The stress tensor is written as follows

$$\mathbf{T} = \begin{bmatrix} \sigma xx & \sigma xy & \sigma xz \\ \sigma yx & \sigma yy & \sigma yz \\ \sigma zx & \sigma xy & \sigma zz \end{bmatrix}. \tag{2.1}$$

The normal stress is given on the diagonal of the stress tensor, whereas the shear stress is stated on the off-diagonal.

Newtons third law states that for every action, there is an equal and opposite reaction. Therefore, the components acting on the same plane, such as σ_{xy} and σ_{yx}, are equal [12].

2.1.2 Strain Tensor

The amount of deformation resulting from stress is called strain, which can be in the form of stretch or compression. Since strain is described as the total displacement of the medium with relation to the initial position, this quantity is unit less. Strain resulting from normal stress is referred to as normal strain. It can be written as

$$\epsilon_{ii} = \frac{\partial u_i}{\partial i}, \tag{2.2}$$

where u is the displacement over an axes and i can be the x, y or z-axis.

The displacement resulting from shear stress is referred to as shear strain. This strain is given by the following expression

$$\epsilon_{ij} = \frac{1}{2}(\frac{\partial u_i}{\partial j} + \frac{\partial u_j}{\partial i}), \tag{2.3}$$

where i $\neq$ j.

Similar to stress, strain is written as a tensor.

$$\varepsilon = \begin{bmatrix} \epsilon_{xx} & \epsilon_{xy} & \epsilon_{xz} \\ \epsilon_{yx} & \epsilon_{yy} & \epsilon_{yz} \\ \epsilon_{zx} & \epsilon_{xy} & \epsilon_{zz} \end{bmatrix}. \tag{2.4}$$

2.1.3 Generalized Hooke's Law

The linear relationship between stress and strain is described by Hooke's law of elasticity. This law is applicable for small stresses and strains [13].
The one-dimensional Hooke's law is given by

$$\varepsilon = \frac{\sigma}{E}, \tag{2.5}$$

where ε is the strain and σ the stress. The modulus of elasticity, E, is a property of isotropic materials, also known as the Young's modulus. This property describes the stiffness of an isotropic material subjected to linear stress.
To extend Hooke's law in three-dimensions, Poisson's Ratio, ν, is introduced. This ratio is defined as the ratio of transverse strain to longitudinal strain, which is applicable for isotropic materials[13].

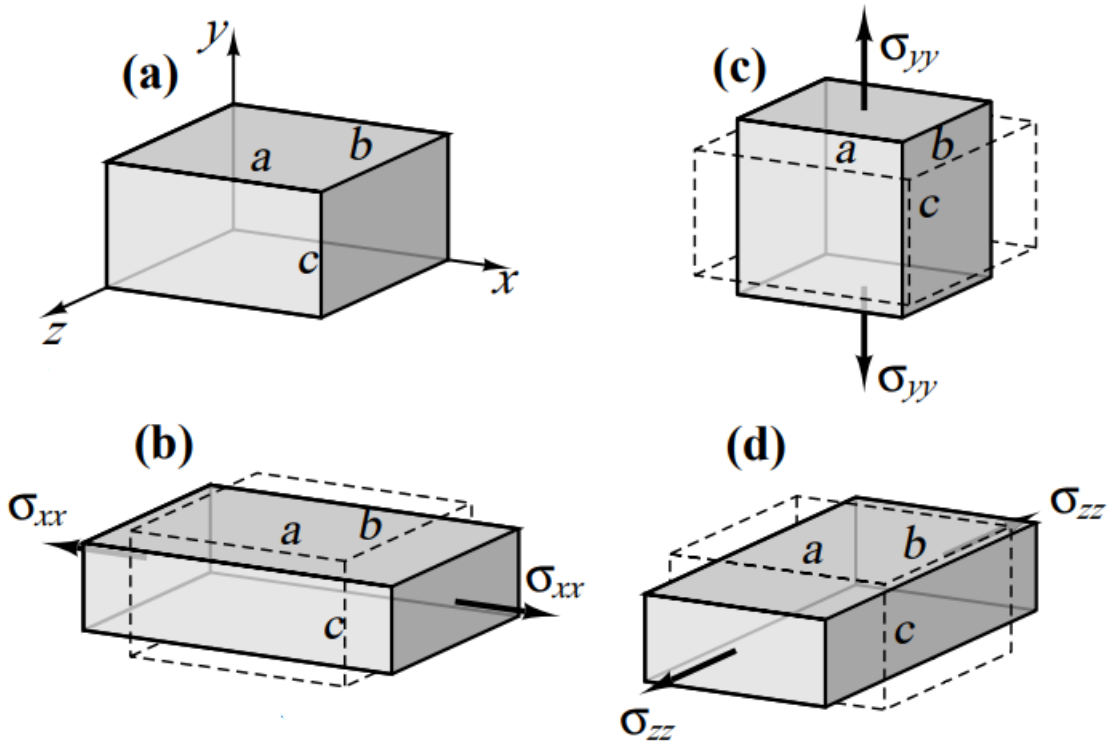

Figure 2.1: Three cases of normal stresses and strains on a three-dimensional cube. (a) is the original shape of the cube [14]

.

In figure 2.1(b) a normal stress is applied on a three-dimensional cube in the x-direction. The stress σ_{xx}, introduces strains in the x, y and z-direction. These strains can be written as

$$\varepsilon'_{xx} = \frac{\sigma_{xx}}{E}, \qquad \varepsilon'_{yy} = -\frac{\nu\sigma_{xx}}{E}, \qquad \varepsilon'_{zz} = -\frac{\nu\sigma_{xx}}{E}. \tag{2.6}$$

In figure 2.1(c) a normal stress is applied in the y-direction. The strains introduced can be written as

$$\varepsilon'_{yy} = \frac{\sigma_{yy}}{E}, \qquad \varepsilon'_{xx} = -\frac{\nu\sigma_{yy}}{E}, \qquad \varepsilon'_{zz} = -\frac{\nu\sigma_{yy}}{E}. \tag{2.7}$$

In figure 2.1(d) a normal stress is applied in the z-direction. The strains introduced can be written as

$$\varepsilon'_{zz} = \frac{\sigma_{zz}}{E}, \qquad \varepsilon'_{xx} = -\frac{\nu\sigma_{zz}}{E}, \qquad \varepsilon'_{yy} = -\frac{\nu\sigma_{zz}}{E}. \tag{2.8}$$

Combining these strains and applying superposition, the following relations are found.

$$\begin{aligned} \varepsilon_{xx} &= \frac{\sigma_{xx}}{E} - \frac{\nu\sigma_{zz}}{E} - \frac{\nu\sigma_{yy}}{E}, \\ \varepsilon_{yy} &= \frac{\sigma_{yy}}{E} - \frac{\nu\sigma_{xx}}{E} - \frac{\nu\sigma_{zz}}{E}, \\ \varepsilon_{zz} &= \frac{\sigma_{zz}}{E} - \frac{\nu\sigma_{xx}}{E} - \frac{\nu\sigma_{yy}}{E}. \end{aligned} \tag{2.9}$$

For the shear stresses and strains, the shear modulus, G, is introduced. This modulus is defined as the ratio of shear stress to shear strain, which is also equal to $G = \frac{E}{2(1+\nu)}$ [14]. The resulting relations are as follows

$$\varepsilon_{xy} = \frac{\sigma_{xy}}{G}, \qquad \varepsilon_{yz} = \frac{\sigma_{yz}}{G}, \qquad \varepsilon_{zx} = \frac{\sigma_{zx}}{G}. \tag{2.10}$$

Combining the equation in 2.9 and 2.10, the following matrix can be constructed.

$$\begin{bmatrix} \varepsilon_{xx} \\ \varepsilon_{yy} \\ \varepsilon_{zz} \\ \varepsilon_{xy} \\ \varepsilon_{yz} \\ \varepsilon_{zx} \end{bmatrix} = \begin{bmatrix} \frac{1}{E} & \frac{-\nu}{E} & \frac{-\nu}{E} & 0 & 0 & 0 \\ \frac{-\nu}{E} & \frac{1}{E} & \frac{-\nu}{E} & 0 & 0 & 0 \\ \frac{-\nu}{E} & \frac{-\nu}{E} & \frac{1}{E} & 0 & 0 & 0 \\ 0 & 0 & 0 & \frac{1}{G} & 0 & 0 \\ 0 & 0 & 0 & 0 & \frac{1}{G} & 0 \\ 0 & 0 & 0 & 0 & 0 & \frac{1}{G} \end{bmatrix} \begin{bmatrix} \sigma_{xx} \\ \sigma_{yy} \\ \sigma_{zz} \\ \sigma_{xy} \\ \sigma_{yz} \\ \sigma_{zx} \end{bmatrix} \tag{2.11}$$

The following expression is obtained when the matrix is inverted.

$$\begin{bmatrix} \sigma_{xx} \\ \sigma_{yy} \\ \sigma_{zz} \\ \sigma_{xy} \\ \sigma_{yz} \\ \sigma_{zx} \end{bmatrix} = \frac{E}{(1-2\nu)(1+\nu)} \begin{bmatrix} 1-\nu & \nu & \nu & 0 & 0 & 0 \\ \nu & 1-\nu & \nu & 0 & 0 & 0 \\ \nu & \nu & 1-\nu & 0 & 0 & 0 \\ 0 & 0 & 0 & \frac{1}{2}-\nu & 0 & 0 \\ 0 & 0 & 0 & 0 & \frac{1}{2}-\nu & 0 \\ 0 & 0 & 0 & 0 & 0 & \frac{1}{2}-\nu \end{bmatrix} \begin{bmatrix} \varepsilon_{xx} \\ \varepsilon_{yy} \\ \varepsilon_{zz} \\ \varepsilon_{xy} \\ \varepsilon_{yz} \\ \varepsilon_{zx} \end{bmatrix} \tag{2.12}$$

Hooke's law can therefore be written in a generalized form

$$\sigma_{ij} = 2\mu\varepsilon_{ij} + \lambda\varepsilon_{ii}\delta_{ij}, \tag{2.13}$$

where μ and λ are Lamé parameters and i and j can be x, y or z [11]. Moreover, δ_{ij} is zero if i≠j. Lamé parameters are defined as follows

$$\mu = G = \frac{E}{2(1+\nu)}, \qquad \lambda = \frac{\nu E}{(1+\nu)(1-2\nu)}. \tag{2.14}$$

2.2 Wave Propagation in Elastic Solids

2.2.1 Equations of Motion

The wave equations in isotropic media can be found by writing Newton's law of motion in terms of stress tensor and displacement, which is done in 2.15.

$$\rho \frac{\partial^2 u_i}{\partial t^2} = \frac{\partial T_{ij}}{\partial x_j} \tag{2.15}$$

Here, ρ is the density of the solid.

Combining 2.15, 2.13, 2.3 and 2.2 the following equation can be found.

$$\rho \frac{\partial^2 u_i}{\partial t^2} = \frac{\partial}{\partial x_j}(\mu(\frac{\partial u_i}{\partial x_j}) + \frac{\partial u_j}{\partial x_i}) + \lambda \frac{\partial u_i}{\partial x_i}\delta_{ij}) \tag{2.16}$$

This equation is rewritten in vectorial form in equation 2.17.

$$\rho \frac{\partial^2 \vec{u}}{\partial t^2} = (\lambda + \mu)\vec{\nabla}(\vec{\nabla} \cdot \vec{u}) + \mu \nabla^2 \vec{u} \tag{2.17}$$

Helmholtz identity states that a vector can be split into both curl of a vector, $\vec{\psi}$, and the gradient of a scalar, ϕ [13]. Therefore, $\vec{u}$ can be written as follows

$$\vec{u} = \vec{\nabla}\phi + \vec{\nabla} \times \vec{\psi}. \tag{2.18}$$

The following rules for scalars and vectors are used

$$\begin{aligned} \vec{\nabla} \times (\vec{\nabla}\phi) &= 0, \\ \vec{\nabla} \cdot (\vec{\nabla} \times \vec{\psi}) &= 0. \end{aligned} \tag{2.19}$$

By combining the equations 2.16, 2.18 and 2.19 the following equation is obtained

$$\vec{\nabla}(\rho \frac{\partial^2 \phi}{\partial t^2} - (\lambda + 2\mu)\nabla^2 \phi) + \vec{\nabla} \times (\rho \frac{\partial^2 \vec{\psi}}{\partial t^2} - \mu \nabla^2 \vec{\psi}) = 0. \tag{2.20}$$

This equation can be separated into a purely scalar equation and a purely vector equation.

$$\begin{aligned} \rho \frac{\partial^2 \phi}{\partial t^2} &= (\lambda + 2\mu)\nabla^2 \phi, \\ \rho \frac{\partial^2 \vec{\psi}}{\partial t^2} &= \mu \nabla^2 \vec{\psi}. \end{aligned} \tag{2.21}$$

The separated equations each describe the propagation of an independent mode. These modes include longitudinal and shear waves. The characteristic of a longitudinal wave is that there is no change in the angle of propagation, which applies to gradient of a scalar (ϕ). For a shear wave, there is no change in volume, which corresponds with the curl of a vector ($\vec{\psi}$) [13]. Shear waves can be polarized in two different direction: horizontal and vertical.

In figure 2.2, the difference between shear waves and longitudinal waves are shown.

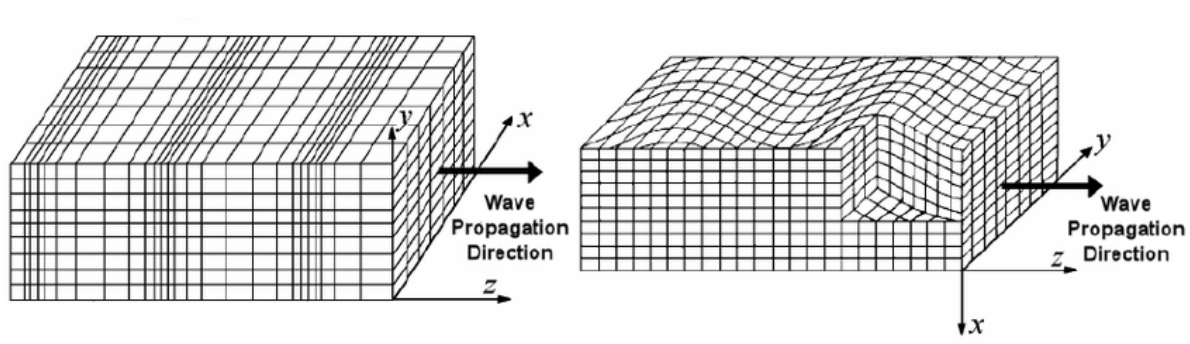

Figure 2.2: Left: the propagation of a longitudinal wave in one dimension. Right: The propagation of a shear wave in one dimension[15]

Knowing that $\vec{u}$ has a longitudinal part ($\vec{u}_L$) and a shear part ($\vec{u}_S$), the equations in 2.21 can be rewritten into the following form

$$\begin{aligned} \frac{\partial^2 \phi}{\partial t^2} &= V_L^2 \nabla^2 \phi, \\ \frac{\partial^2 \vec{\psi}}{\partial t^2} &= V_S^2 \nabla^2 \vec{\psi}, \end{aligned} \tag{2.22}$$

with V_L the bulk velocity of the longitudinal wave and V_S the bulk velocity of the shear waves. These parameters are defined as follows

$$V_L^2 = \frac{\lambda + 2\mu}{\rho}, \qquad V_S^2 = \frac{\mu}{\rho}. \tag{2.23}$$

Knowing $\vec{\psi}$ is a vector with the x, y and z-components, the wave equations in 2.22 can be extended rewritten in the following form

$$\begin{aligned} \frac{1}{V_L^2}\frac{\partial^2 \phi}{\partial t^2} &= \frac{\partial^2 \phi}{\partial x^2} + \frac{\partial^2 \phi}{\partial y^2} + \frac{\partial^2 \phi}{\partial z^2}, \\ \frac{1}{V_S^2}\frac{\partial^2 \psi_x}{\partial t^2} &= \frac{\partial^2 \psi_x}{\partial x^2} + \frac{\partial^2 \psi_x}{\partial y^2} + \frac{\partial^2 \psi_x}{\partial z^2}, \\ \frac{1}{V_S^2}\frac{\partial^2 \psi_y}{\partial t^2} &= \frac{\partial^2 \psi_y}{\partial x^2} + \frac{\partial^2 \psi_y}{\partial y^2} + \frac{\partial^2 \psi_y}{\partial z^2}, \\ \frac{1}{V_S^2}\frac{\partial^2 \psi_z}{\partial t^2} &= \frac{\partial^2 \psi_z}{\partial x^2} + \frac{\partial^2 \psi_z}{\partial y^2} + \frac{\partial^2 \psi_z}{\partial z^2}. \end{aligned} \tag{2.24}$$

From equation 2.18, the following equations of the general wave motion can be found

$$\begin{aligned} u_x &= \frac{\partial \phi}{\partial x} + \frac{\partial \psi_z}{\partial y} - \frac{\partial \psi_y}{\partial z}, \\ u_y &= \frac{\partial \phi}{\partial y} + \frac{\partial \psi_x}{\partial z} - \frac{\partial \psi_z}{\partial x}, \\ u_z &= \frac{\partial \phi}{\partial z} + \frac{\partial \psi_y}{\partial x} - \frac{\partial \psi_x}{\partial y}. \end{aligned} \tag{2.25}$$

2.3 Plane Waves

Plane waves are three dimensional waves with the normal vector parallel to the z-axis. The two waves that propagate in an isotropic solid plate are Lamb waves and shear horizontal waves [16] .

2.3.1 Boundary Conditions

In the case of a traction free plate, with a finite thickness of $z = \pm h$ and invariance in the y-direction, the following conditions apply[12]

$$\begin{aligned} \frac{\partial}{\partial y} &= 0, \\ \nabla &= \frac{\partial}{\partial x}\hat{i} + \frac{\partial}{\partial z}\hat{k}. \end{aligned} \tag{2.26}$$

The invariance in the y-direction is the result of the plain strain conditions, which states that stresses and strains only have non-zero components in a single plane [17]. Applying these conditions to the wave motions in 2.25, the following expression is obtained

$$\vec{u} = (\frac{\partial \phi}{\partial x} - \frac{\partial \psi y}{\partial z})\hat{i} + (\frac{\partial \psi x}{\partial z} - \frac{\partial \psi z}{\partial x})\hat{j} + (\frac{\partial \phi}{\partial z} + \frac{\partial \psi y}{\partial x})\hat{k}. \tag{2.27}$$

The x-component and the z-component of this wave motion vector depends on the longitudinal wave motion, ϕ, and vertically polarized shear wave motion, ψy. The y-component in this vector describes the horizontal polarized shear wave, which depends on ψz and ψx. Since the shear horizontal wave does not depend on ψy or ϕ, it is completely decoupled from the lamb waves.

2.3.2 Lamb Waves

Lamb wave equations consist of two waves, the longitudinal wave and the vertically polarized shear wave[16].
The boundary conditions for this wave are [18]

$$\begin{aligned} \sigma_{zz} = \sigma_{xz} &= 0, \\ u_y &= 0, \\ \frac{\partial}{\partial y} &= 0. \end{aligned} \tag{2.28}$$

These boundary conditions result in the reduction of the wave motion vector in 2.27. The components for the wave motion of lamb waves are as follows

$$\begin{aligned} u_x &= \frac{\partial \phi}{\partial x} - \frac{\partial \psi y}{\partial z}, \\ u_z &= \frac{\partial \phi}{\partial z} + \frac{\partial \psi y}{\partial x}. \end{aligned} \tag{2.29}$$

Lamb waves consist of waves standing in the z-direction and propagating in the x direction. Therefore, the lamb waves are described by the following two-dimensional wave equations

$$\begin{aligned} \frac{1}{V_L^2}\frac{\partial^2 \phi}{\partial t^2} &= \frac{\partial^2 \phi}{\partial x^2} + \frac{\partial^2 \phi}{\partial z^2}, \\ \frac{1}{V_S^2}\frac{\partial^2 \psi y}{\partial t^2} &= \frac{\partial^2 \psi y}{\partial x^2} + \frac{\partial^2 \psi y}{\partial z^2}. \end{aligned} \tag{2.30}$$

The resulting stress components from the plain strain can be obtained using 2.15 and 2.29.

$$\begin{aligned}\sigma_{xx} &= \lambda\left(\frac{\partial^2\phi}{\partial x^2}+\frac{\partial^2\phi}{\partial z^2}\right)+2\mu\left(\frac{\partial^2\phi}{\partial x^2}-\frac{\partial^2\psi_y}{\partial x\partial z}\right),\\ \sigma_{zz} &= \lambda\left(\frac{\partial^2\phi}{\partial x^2}+\frac{\partial^2\phi}{\partial z^2}\right)+2\mu\left(\frac{\partial^2\phi}{\partial z^2}+\frac{\partial^2\psi_y}{\partial x\partial z}\right),\\ \sigma_{xz} &= \mu\left(2\frac{\partial^2\phi}{\partial x\partial z}+\frac{\partial^2\psi_y}{\partial x^2}-\frac{\partial^2\psi_y}{\partial z^2}\right).\end{aligned} \tag{2.31}$$

The solution for the wave equation 2.30 will have the following form

$$\begin{aligned}\phi &= \Phi(z)e^{j(kx-\omega t)},\\ \psi_y &= \Psi(z)e^{j(kx-\omega t)}.\end{aligned} \tag{2.32}$$

where ω is the angular frequency and k the wavenumber. Combining equation 2.30 and 2.32 give the following expressions

$$\begin{aligned}\frac{\partial^2\Phi}{\partial z^2}+\alpha^2\phi=0,\\ \frac{\partial^2\Psi}{\partial z^2}+\beta^2\psi=0,\end{aligned} \tag{2.33}$$

where α and β are defined as follows

$$\alpha^2=\frac{\omega^2}{V_L^2}-k^2, \qquad \beta^2=\frac{\omega^2}{V_S^2}-k^2. \tag{2.34}$$

Solving the equations in 2.33 give the following expressions

$$\begin{aligned}\Phi(z) &= Asin(\alpha z)+Bcos(\alpha z),\\ \Psi(z) &= Csin(\beta z)+Dcos(\beta z).\end{aligned} \tag{2.35}$$

There are two modes of wave propagation: the symmetric mode and the antisymmetric mode. The displacement in the x-direction is symmetric, with regard to the z-axis, if the solution contains cosines and the displacement in the z-direction is symmetric, with regard to the z-axis, if the solution contains sines[12].

Therefore, the symmetric mode is given by the following system

$$\begin{aligned}\Phi &= Bcos(\alpha z), \qquad \Psi = Csin(\beta z),\\ u_x &= ikBcos\left(\alpha z\right)-\beta Ccos\left(\beta z\right),\\ u_z &= B\alpha sin\left(\alpha z\right)+Ciksin\left(\beta z\right),\\ \sigma_{xx} &= -\lambda\left(k^2+\alpha^2\right)Bcos\left(\alpha z\right)+2\mu\left(ik\beta Ccos\left(\beta z\right)-k^2Bcos\left(\alpha z\right)\right),\\ \sigma_{zz} &= -\lambda\left(k^2+\alpha^2\right)Bcos\left(\alpha z\right)+2\mu\left(ik\beta Ccos\left(\beta z\right)-\alpha^2Bcos\left(\alpha z\right)\right),\\ \sigma_{xz} &= -\mu\left[2\alpha ikBsin\left(\alpha z\right)+\left(k^2-\beta^2\right)Csin\left(\beta z\right)\right].\end{aligned} \tag{2.36}$$

The antisymmetric mode is given by the following system

$$\begin{aligned}
\Phi = Asin(\alpha z), \qquad \Psi = Dcos(\beta z),\\
u_x = ikAsin\left(\alpha z\right) + \beta Dsin\left(\beta z\right),\\
u_z = \alpha Acos\left(\alpha z\right) + ikDcos\left(\beta z\right),\\
\sigma_{xx} = -\lambda\left(k^2+\alpha^2\right)Asin\left(\alpha z\right) - 2\mu\left(ik\beta Dsin\left(\beta z\right) + k^2 Asin\left(\alpha z\right)\right),\\
\sigma_{zz} = -\lambda\left(k^2+\alpha^2\right)Asin\left(\alpha z\right) - 2\mu\left(ik\beta Dsin\left(\beta z\right) + \alpha^2 Asin\left(\alpha z\right)\right),\\
\sigma_{xz} = \mu\left[2\alpha ikAcos\left(\alpha z\right) + \left(\beta^2 - k^2\right)Dcos\left(\beta z\right)\right].
\end{aligned} \tag{2.37}$$

Combining the boundary condition for stress in 2.28, the symmetric σ_{zz} and the symmetric σ_{xz} in 2.36, the following frequency equation can be formed

$$\left(k^2-\beta^2\right)^2 cos\left(\alpha h\right) sin\left(\alpha h\right) + 4k^2\alpha\beta sin\left(\alpha h\right) cos\left(\beta h\right) = 0. \tag{2.38}$$

This can be rewritten in the following form

$$\frac{tan\left(\beta h\right)}{tan\left(\alpha h\right)} = \frac{-4k^2\alpha\beta}{\left(k^2-\beta^2\right)^2}. \tag{2.39}$$

This equation is known as the Rayleigh-Lamb frequency equation for symmetric waves in a plate[12]. The Rayleigh-Lamb frequency equation for antisymmetric waves in a plate is given as follows

$$\frac{tan\left(\beta h\right)}{tan\left(\alpha h\right)} = \frac{-\left(k^2-\beta^2\right)^2}{4k^2\alpha\beta}. \tag{2.40}$$

2.3.3 Shear Horizontal Waves

The second type of wave in a plane wave are shear waves polarized in the horizontal direction (SH-waves). This wave propagates in the x-direction with a standing wave in the y-direction.

Since SH-waves only depend on the y-component, the wave motion vector in 2.27 can be reduced to the following equation[17]

$$u_y = \frac{\partial\psi_x}{\partial z} - \frac{\partial\psi_z}{\partial x}. \tag{2.41}$$

The wave equation, for SH-waves, is as follows

$$\frac{1}{V_S^2}\frac{\partial^2 u_y}{\partial t^2} = \frac{\partial^2 u_y}{\partial x^2} + \frac{\partial^2 u_y}{\partial z^2}. \tag{2.42}$$

The solution of the wave equation will have the following form

$$u_y = h(z)e^{j(kx-\omega t)}. \tag{2.43}$$

Combining equation 2.43 and equation 2.42, the following expression can be found

$$\frac{\partial^2 h(z)}{\partial z^2} + \eta^2 h(z) = 0, \tag{2.44}$$

where η is defined as follows

$$\eta^2 = \frac{\omega^2}{V_S^2} - k^2. \tag{2.45}$$

Solving equation 2.44 gives

$$h(y) = C_1 cos(\eta z) + C_2 sin(\eta z). \tag{2.46}$$

Therefore, equation 2.43 can be written as

$$u_y = (C_1 cos(\eta z) + C_2 sin(\eta z)) e^{j(kx-\omega t)}. \tag{2.47}$$

The boundary conditions of SH-waves at the surface z = ± h, are as follows [16]

$$\begin{aligned} \sigma_{zz} = \sigma_{xz} = \sigma_{yz} = 0, \\ \frac{\partial u_y}{\partial z} = 0. \end{aligned} \tag{2.48}$$

Applying these conditions to 2.47 gives the following equation

$$\begin{aligned} C_1 cos(\eta h) + C_2 sin(\eta h) = 0, \\ C_1 cos(\eta h) - C_2 sin(\eta h) = 0. \end{aligned} \tag{2.49}$$

Solving these equations leads to the following frequency equation

$$cos(\eta h) sin(\eta h) = 0. \tag{2.50}$$

This equation satisfies equation 2.51 in case of symmetric modes

$$\eta h = n\pi, \qquad n = 0, 1, 2, ... \tag{2.51}$$

For antisymmetric modes, equation 2.50 satisfies the following equation

$$\eta h = (2n+1)\frac{\pi}{2}, \qquad n = 0, 1, 2, ... \tag{2.52}$$

The dispersion relation for symmetric modes can therefore be rewritten as follows,

$$k^2 = \left(\frac{\omega^2}{V_S^2}\right)^2 - \left(\frac{n\pi}{h}\right)^2, \tag{2.53}$$

where n is the mode index.

2.4 Ultrasonic Non-Destructive Testing

Ultrasonic non-destructive testing (NDT) is a method where the thermodynamic properties of a fluid can be evaluated without causing damage to the equipment. This report focuses on the method of NDT using an immersed waveguide and a piezoelectric transducer. Using a waveguide allows the transducer to be protected from high temperature and high corrosive environment.

For measuring the viscosity of a fluid, the attenuation of the transmitted wave, inside the waveguide, should be evaluated with non-dispersive waves[7].

2.4.1 Attenuation

The attenuation of a wave describes the loss or absorption of the wave energy by the medium. For longitudinal waves, the attenuation depends mainly on the viscosity and the thermodynamic properties of the fluid. In contrary to solids, shear waves do not exist in fluids and gases, due to the absence of shape elasticity[11]. Therefore, the attenuation for shear waves is mainly determined by leaking waves at the surface of the solid and dissipation and scattering of the wave energy[19].

In Appendix A the behavior of longitudinal waves in a fluid is described. In equation A.12, the attenuation for longitudinal wave is determined to have the following expression

$$\alpha_{long} = \frac{2\upsilon\omega^2}{3V_0^3}. \tag{2.54}$$

where, υ is the kinematic viscosity of the fluid.

For shear waves the attenuation is acquired by dividing the energy leakage across the boundary of the waveguide by the average power flow across the cross section of the waveguide [19].

In case of the shear horizontal waves, the energy leakage is defined as the integral of power flow over unit width of the plate. Using the Pointing vector for finding the the average power flow, the following equation for the attenuation (α_{SH}) can be found [19]

$$\alpha_{SH} = -\frac{1}{2h}\left(\frac{\rho_0\omega\eta}{\rho G}\right)^{\frac{1}{2}}, \tag{2.55}$$

where h is the width of the plate and η the dynamic viscosity of the fluid.

For ultrasonic NDT, high frequency signals with non-dispersive ultrasonic waves are needed. Dispersion introduces multiple modes and attenuation[7]. For accurate evaluation of the viscosity, the attenuation should primarily be introduced by the immersion fluid. Therefore, it is desirable to transmit a non-dispersive signal into the waveguide[7].

2.4.2 Non-Dispersive SH0 Waves

A non-dispersive signal should have a constant wave velocity independent of frequency[8]. The wave velocity can be found from the dispersion relation, where the angular frequency is dependent on the wave number.

There are two kinds of wave velocities: phase velocity (V_{phase}) and group velocity (V_{group}). The group velocity gives the velocity of the wave package, whereas the phase velocity gives the velocity of an individual peak within the overall wave shape. In figure 2.3 the difference between the two velocities can be seen.

The expression for the phase velocity and group velocity can be seen in the following equation

$$V_{phase} = \frac{\omega}{k}, \qquad V_{group} = \frac{\partial\omega}{\partial k}. \tag{2.56}$$

In figure 2.3, the green dot follows the overall shape of the function, which will give V_{group}, and the red do follows a single phase, which will give V_{phase}.

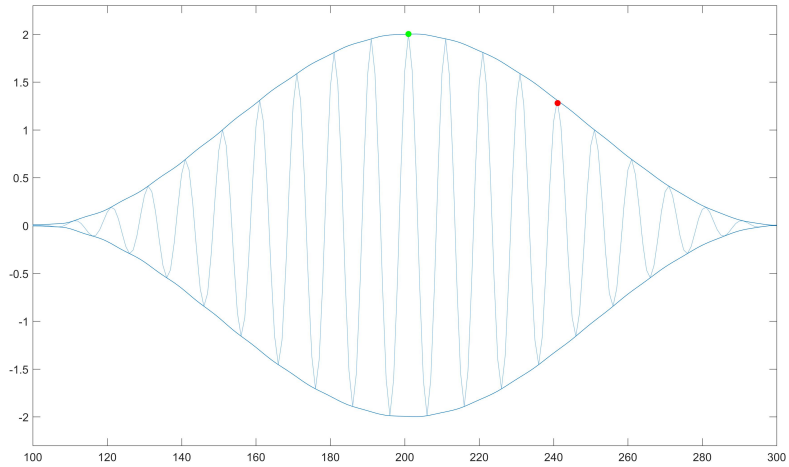

Figure 2.3: An analytic envelope function over a signal. The green dot follows the overall shape of the function and the red do follows a single phase.

To create a non-dispersive signal, the group velocity of shear horizontal waves will be evaluated.

Using the dispersion relation in equation 2.53 and equation 2.56, the group velocity of shear horizontal waves can found

$$V_{group} = V_S \sqrt{1 - \left(\frac{nV_S}{2fh}\right)^2}, \tag{2.57}$$

where f is the signal frequency, h is the thickness of the plate and n the mode of the wave. The first mode of the shear horizontal waves, SH0 with n=0, is independent of frequency and therefore non-dispersive.

From equation 2.57, the following dispersion curve can be obtained.

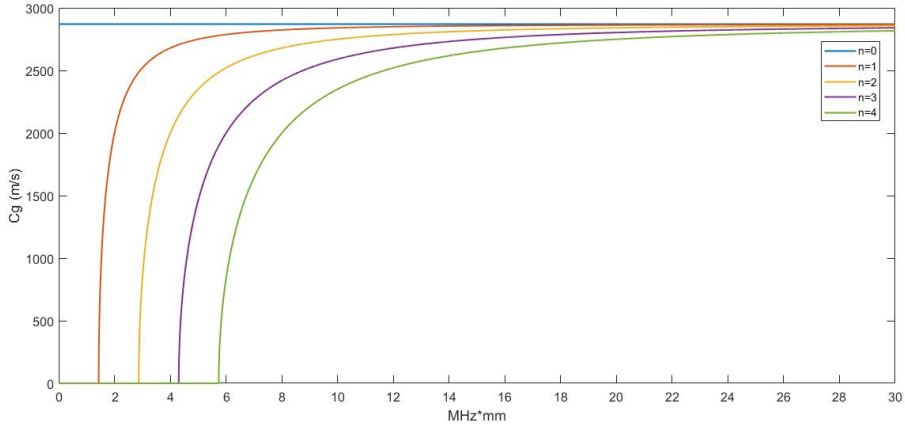

Figure 2.4: The group velocity, in m/s, for a tungsten plate plotted against the the frequency of the pulse times the thickness of the plate in MHZ·mm

Since non-dispersive wave modes are preferred for measurements, the other modes should be filtered out using the cut-off frequency thickness (f_h).

To exclude these other wave modes, using the thickness of the plate, equation 2.57 is used to define the following cutoff frequency thickness product.

$$f_h = \frac{V_S}{2} MHz \cdot mm. \tag{2.58}$$

The frequency used for non-destructive inspection, range from 1 MHz to 5 MHz [7].

The bulk shear velocity, given for the SH0 mode, only apply for infinite plates. For a plate with finite width, the group velocity asymptotically approaches the shear bulk velocity above a certain critical cut-off frequency width product (f_w). If the frequency width product of a plate is smaller than the critical f_w, the signal will be dispersed [8]. To find this value, the peak time for different plate width dimensions should be evaluated.

Chapter 3

Experimental Method

In this chapter the experimental method is described. In the first section, a detailed description of the waveguide model is given. The model is build in the finite element software COMSOL[20].

The steps for finite element data post processing are stated in in the second section. Post processing include: obtaining the group velocity and the attenuation.

3.1 The Wave Guide Model

The standard steps for modeling in COMSOL include: specifying definitions, geometry, materials, physics, mesh, study and progress the results.

3.1.1 Geometry and Definitions

For the waveguide immersed in water, a workplace with a rectangle and a block are created with the *geometry toolbar*. The rectangle will simulate the waveguide and the block will simulate the fluid. For this model the plate is a 2D object, since 3D can be computationally expensive. In the figure below, the resulting geometry can be seen.

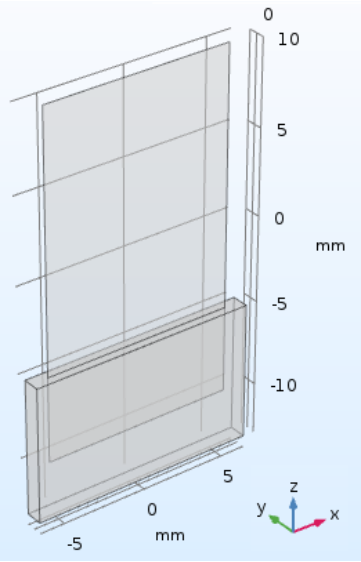

Figure 3.1: The geometry created in COMSOL.

To define the boundaries of the transducer, two points are made. The length between the points will be the diameter of the transducer. In figure 3.2, the workspace with the two points is shown.

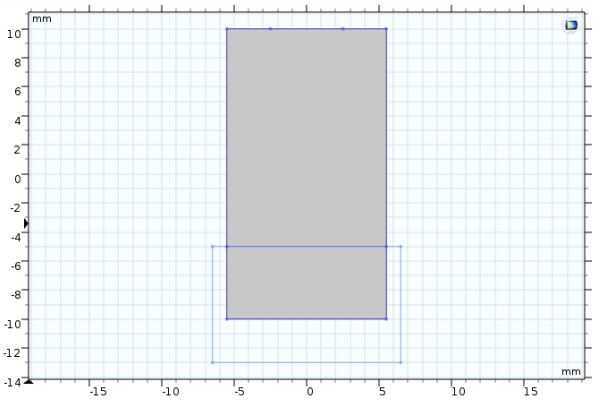

Figure 3.2: The 2D workspace created in COMSOL.

The dimensions of this geometry are given in the *Parameters*, which can be found in Appendix A. The dimensions of the plate are smaller than the actual size of the wavelength. To minimize the computation time, the dimensions are scaled down.

To organize the model, the function *Explicit* in the *Definitions toolbar* is used to define the fluid domain and the solid boundary. Moreover, the input edge for the pulse is defined, which is the space between the two points.

The materials used are chosen from the *Build-In Materials* available in COMSOL. For the liquid domain, *Water,liquid* is chosen and for the solid domain: *Tungsten*. The metal Tungsten, also known as Wolfram, is a commonly used material in high temperature and radioactive environments, due to its high melting point and high density[21]. In table 3.1, the parameters, used in this model, for tungsten are given.

Table 3.1: The material properties of Tungsten[20].

Parameters	Values
Density (kg m^{-3})	17800
Lamé's constant, λ (GPa)	179
Lamé's constant, μ (GPa)	141
Poisson ratio, υ	0.28
Young's modulus, E (GPa)	360
Thermal conductivity (W m^{-1} K^{-1})	175
V_L (m s^{-1})	5089
V_S (m s^{-1})	2814

In table 3.1, V_L and V_S are calculated using equation 2.23.

3.1.2 Physics

The model uses 'Thermoviscous Acoustics, Transient', 'Shell' and the multiphysics 'Thermoviscous Acoustic - Structure Boundary' to model ultrasonic shear horizontal waves in a waveguide made from Tungsten.

Thermoviscous acoustics is a computationally expensive interface and will take viscous and thermal losses into account. For larger models, the *Pressure Acoustics* interface with the fluid model set to *Thermally conducting and viscous* can be used to reduce computation time[22].

Since, thermoviscous acoustics is computationally expensive, the plate is modeled using the 2D shell physics. The shell physics is for thin plates made from a material with significant bending stiffness[23], which applies for the metal tungsten. This shell physics provides the ability to simulate a 3D plate with a small thickness in 2D.

To simulate a acoustic pulse, the function *Prescribed Displacement* is used in the *Physics toolbar*. In this research a sinus wave with 5 cycles, an amplitude of 0.1 V and a pulse frequency of 2MHz, is implemented as input pulse. The resulting pulse can be seen in figure 3.3. To generate this input pulse, the piecewise function in COMSOL is utilized.

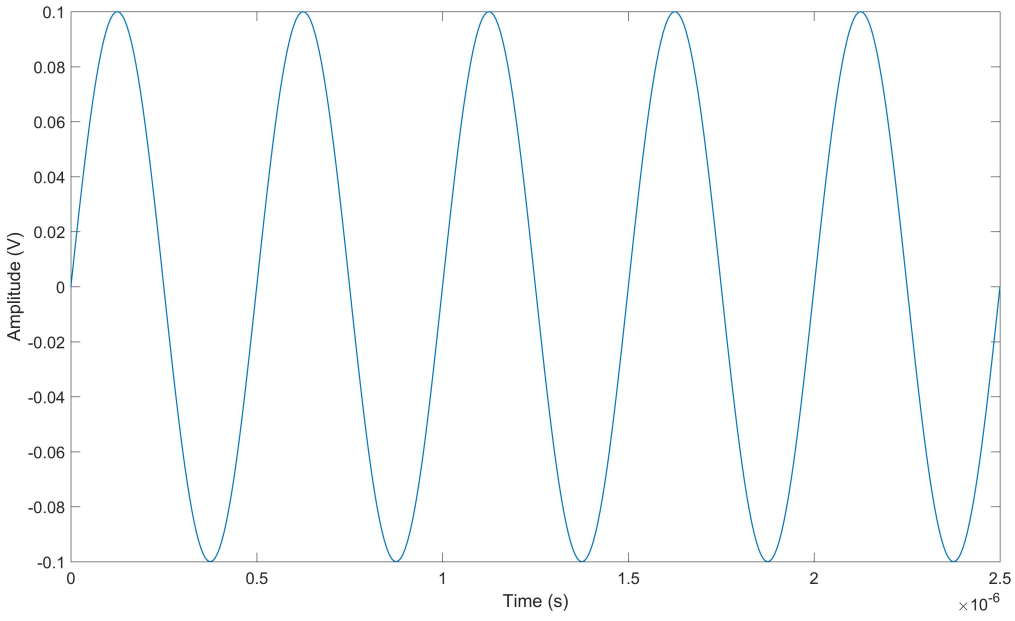

Figure 3.3: A 5-cycle sin pulse with a pulse frequency of 2MHz and an amplitude of 0.1 V.

Since the desired wave for this experiment is the shear horizontal wave, the pulse is send into the x-direction.

3.1.3 Mesh

For the mesh size it is important to take the Nyquist criterion into account, which stated there should be at least two mesh elements per wavelength. In previous research, the optimal amount of mesh elements per wavelength was found to be eight[9]. Therefore, this is also the amount of mesh elements per wavelength in this model.

Since the exited shear horizontal wave only causes displacement, for the plate, in the x-direction, it is preferred to use square mesh elements. Therefore, for the 2D plate, the mapped mesh is used. For the mapped mesh the distribution can be specified.

An example of a distribution, is the inverse Gaussian distribution. This distribution increases the resolution of the model at the edges of the plate, which might be more beneficial for shear horizontal wave measurements[24]. However, combining this distribution with the computationally expensive 'Thermoviscous Acoustics' interface will increase the computation time significantly.

To minimize the computation time of this model, the mapped mesh is equally distributed over the plate.

In the fluid domain, the free tetrahedral mesh is implemented. In figure 3.4 the resulting mesh is shown.

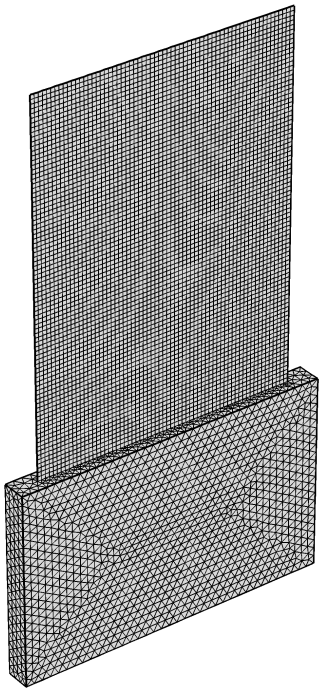

Figure 3.4: The mesh used for the model.

In figure 3.5, a zoomed in version of figure 3.4 can be seen.

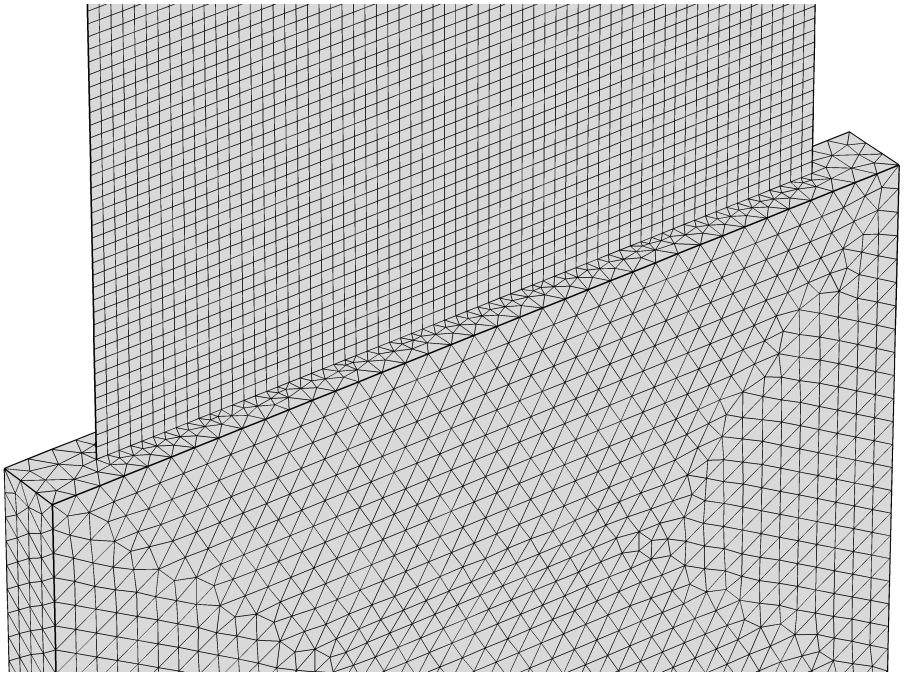

Figure 3.5: The mesh used for the model.

The size of mesh elements is calculated with the following equation

$$M = \frac{\lambda_{SH}}{N}, \tag{3.1}$$

where M is the mesh size, N is the amount of mesh elements per wavelength and λ the wavelength of shear horizontal ultrasonic waves.

3.1.4 Study

For this simulation the *Time Dependent study* is chosen, which requires a start time, end time and step size. The distance that the information travels within the time step must be smaller than the mesh size, for the simulation to converge. This condition is also known as the Courant-Friedrichs-Lewy (CFL) condition[25]. The time step is therefore calculated with the following equation

$$t_{step} = CFL\frac{\lambda_{SH}}{V_{SH}N} = \frac{CFL}{f_0 N}, \tag{3.2}$$

where CFL is the optimal scaling factor and f_0 is the frequency of the excited pulse.

The CFL number is a positive, nonzero value, which should be less than 0.2[26].

When the simulation is started, the solver will automatically define the time steps taken by the solver by interpolation. This works perfectly for predictable signals. However, for sudden changes in the signal or oscillations, the automatic solver will end up under-sampling the solution. Therefore, it is recommended to set *Steps taken by Solver* to *Manual*.

3.2 Post processing

To obtain the data after computing, a point evaluation is implemented. For this point, the second Piola-Kircho stress tensor (component xz) is used to obtain the displacement, resulting from the shear

horizontal wave.

3.2.1 Group Velocity and Attenuation

For calculating group velocity the following equation is used

$$V_{group} = \frac{2L}{\Delta t}, \tag{3.3}$$

where L is the length of the plate and Δt the time delay of the returning peak.

To efficiently calculate the time delay of the returning pulse, the cross correlation function can be utilized. This function measures the similarities between two pulses. In figure 3.6, an example of an input pulse and a returning pulse are shown.

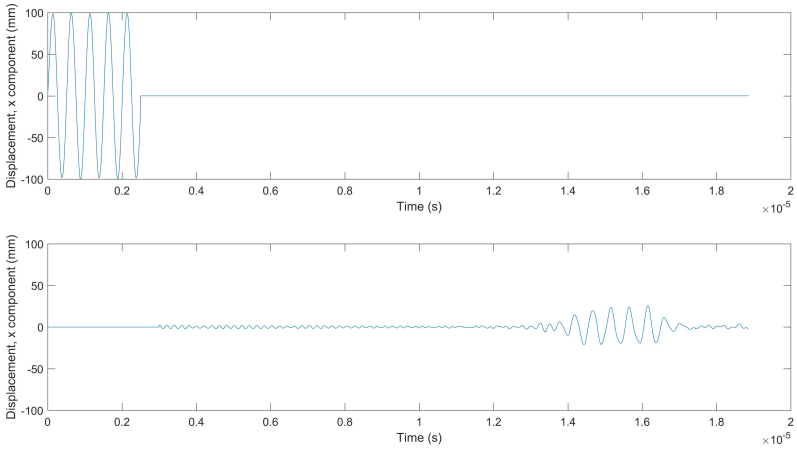

Figure 3.6: The upper plot shows the input pulse of a 5-cycle sinusoidal wave and the lower plot the returning pulse.

The cross correlation between the two pulses in figure 3.6, gives the following output in figure 3.7.

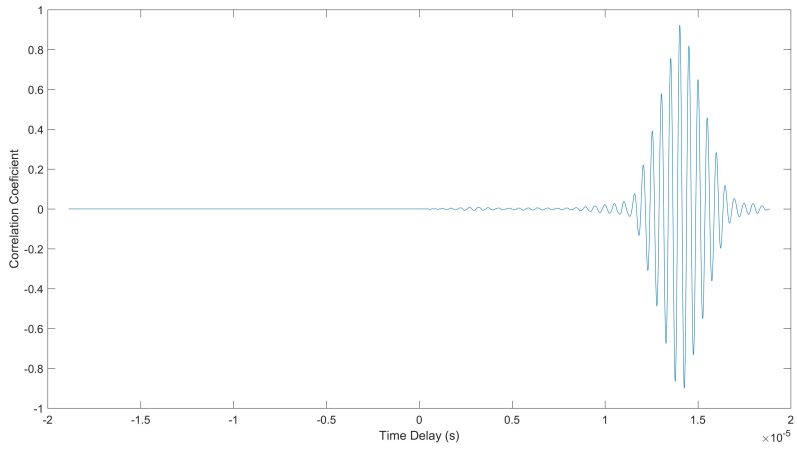

Figure 3.7: The cross correlation coefficient plotted against the time delay of the pulse.

The maximum of the cross correlation function returns the delay of the echo, also known as lag. In

Matlab this delay is expressed in number of samples and can be expressed in time by dividing this delay by the total number of samples.

When a shear horizontal wave is excited, it travels through the plate and is reflected back at the solid-fluid surface. While traveling though the plate, the pulse losses energy due to the attenuation of the waveguide itself and the attenuation introduced by the fluid.

A returning signal, or echo, in an immersed plate will have a slight delay compared to the echo in the plate which is slightly less immersed. This delay will hold information about the attenuation of the fluid in which the plate is immersed.

The amplitude of the returning signal in the waveguide, $S(\omega)$, is characterized by the following exponential decrease

$$S(\omega) = RS_0(\omega)e^{-2x\alpha_{fluid}}e^{-2x\alpha_{waveguide}}, \tag{3.4}$$

where R is the reflection coefficient for the fluid-solid interface at the bottom of the waveguide, $S_0(\omega)$ the initial signal strength, x the immersion depth, α_{fluid} is the total attenuation per meter introduced by the fluid and $\alpha_{waveguide}$ is the total attenuation per meter introduced by the waveguide. The expression for R can be found in appendix B.

By measuring the time delay and amplitude for two different immersion depths, the relationship between attenuation and immersion depth can be found. The parameters such as R, $\alpha_{waveguide}$ and S_0, are identical for both measurements and will vanish by equating the identical parameters of the two measurements. The following equation for the attenuation can be found [19]

$$\alpha_{fluid} = -\frac{1}{2\left(x_2 - x_1\right)} ln\left(\frac{S_2(\omega)}{S_1(\omega)}\right), \qquad for:\ x_2 < x_1, \tag{3.5}$$

where α_{fluid} is the attenuation, x_2 and x_1 are different immersion depths and S_1 and S_2 are the different signal amplitude at the different immersion depths. For equation 3.5, the Fourier transform of the amplitude is used to counter the effects of dispersion[19].

When using shear horizontal ultrasonic waves, the attenuation acquired with equation 3.5 can be used in equation 2.55 to calculate the dynamic viscosity of the fluid.

For estimating the accuracy of the model the Matlab functions 'mean' and 'std' are used for calculating the mean and standard deviation of a vector[27].

Chapter 4

Results and Discussion

In this chapter the results of the model are stated. At first, the optimal plate width dimension, for the shear horizontal waves, is determined with the model.

Secondly, the model is optimized for the time step size of the solver. For both studies, the accuracy of the model is studied by comparing the group velocity, calculated by the model, to the theoretical group velocity of tungsten.

4.1 Plate Dimensions

For optimizing the plate width, the model is studied without the immersion fluid to minimize the solving time. The plate has a length of 20 mm and a thickness of 0.1 mm and the material of the plate is Tungsten. The transducer on top of the plate has a width of 4.8 mm and sends a 5-cycle sinus pulse into the plate with an amplitude of 0.1 m and a frequency of 2 MHz. For the mesh, a size of 8 mesh elements per wavelength is used. As discussed in the previous chapter, the optimal scaling factor (CFL number) should be positive, nonzero and smaller than 0.2. For now, the CFL number is set to 0.1.

4.1.1 Parametric sweep

The cut-off frequency width is determined by a parameter sweep for the plate width values; 5 mm to 15 mm in steps of 1 mm.

The results of the parametric sweep can be seen in the figure below

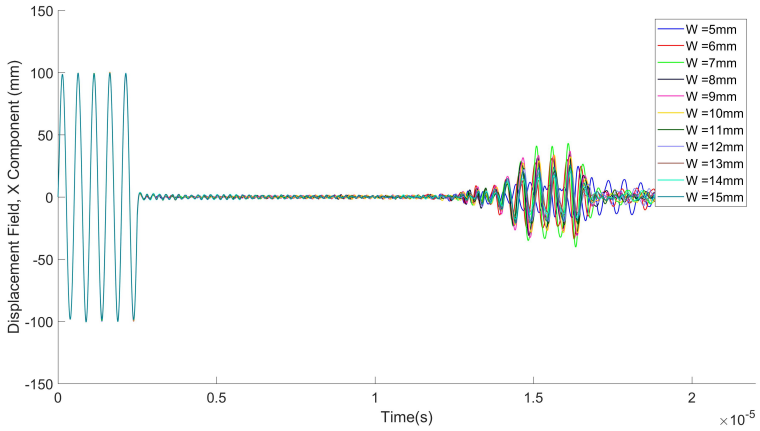

Figure 4.1: The SH0 wave measured on top of the waveguide for different plate width's. Displacement field in the x-direction plotted again the time. Measured with a boundary point probe.

In figure 4.1, there are three peaks that seem to change a lot for every different plate width, the first of these three, around 15.2 μs, is evaluated. In figure 4.2, the echo of the pulse can be seen for different plate width dimensions.

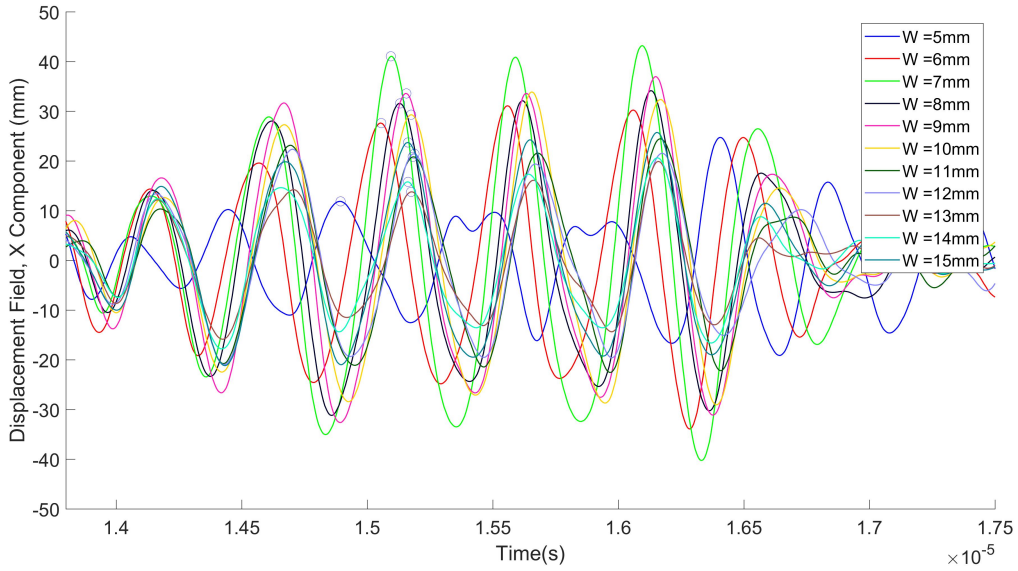

Figure 4.2: The SH0 wave measured on top of the waveguide for different plate width's. Displacement field in the x-direction plotted again the time. The evaluated peaks are marked with a circle.

In figure 4.1 and figure 4.2, it can be seen that for the width of 5 mm the returned signal is fully dispersed. This is an indication that the critical cut-off frequency width is 12 MHz·mm, i.e., the plate should be at least 6 mm for a pulse frequency of 2 MHz.

The wider the plate, the more the wave is distributed over the plate. Therefore, the amplitude decreases as the plate width increases. To determine the optimal plate width, the peak time is evaluated. The results can be found in the table below.

Table 4.1: The values of the width of the plate with the corresponding peak time of the returning shear horizontal wave.

Width (mm)	Peak Time (μs)
5	14.8940
6	15.0560
7	15.0940
8	15.1310
9	15.1560
10	15.1750
11	15.1810
12	15.1880
13	15.1750
14	15.1630
15	15.1630

In figure 4.3, the values from table 4.1 are plotted.

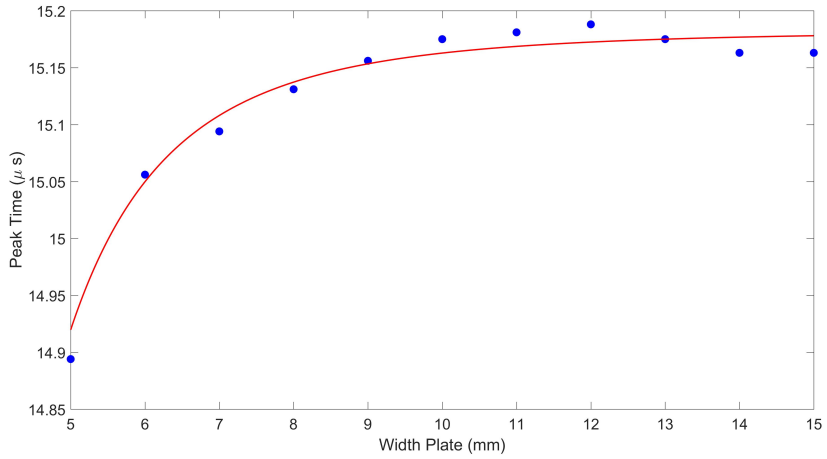

Figure 4.3: The peak time of the returning shear horizontal wave plotted against the width of the plate.

In figure 4.3, the fitted line is the following power function

$$y(x) = ax^b + c \tag{4.1}$$

where a = -109.9 ± 514.4 , b = -3.751 ± 2.626 and c = 15.18 ± 0.02. Since a plate width of 5 mm does not give a reasonable solution for the returning echo, this data point is disregarded in the fitted line.

In figure 4.3, the optimal frequency width product lies around 20 MHz·mm. It can also be seen that the peak times do not seem to stabilize for a single peak time but rather oscillate around 15.17 μs. The cause of this oscillation can be either a natural phenomena or, more likely, a numerical problem in the model. By increasing the resolution of the model, the numerical problems can be minimized. However, increasing the resolution, will also increase the computation time. Since the oscillation is relatively small, the contributing factors of this oscillation can be disregarded in this research.

4.1.2 Accuracy

To study the accuracy of the results, the group velocity of the pulse, measured by the model, is compared to the theoretical value. To obtain the group velocity, the time delay is calculated using the cross correlation function.

The mean value of the time delay, for the width study, was calculated to be 14.13 ± 0.11 μs, where 0.11 is the standard deviation. For calculating this mean value, the data point at W = 5 mm is disregarded.
The values of the time delay, resulting from the cross correlation function, can be found in table 4.2.

Table 4.2: The value for the time delay for every plate width.

Width (mm)	Time Delay (μs)
5	15.9937
6	14.1563
7	14.2062
8	14.2375
9	14.2625
10	14.2813
11	14.0500
12	14.0500
13	14.0375
14	14.0188
15	14.0250

With equation 3.3, the group velocity is calculated. The resulting values, for the group velocity, can be seen in table 4.3.
The mean value for the group velocity is calculated to be equal to 2830 ± 21 m s^{-1}, where $\pm$ 21 is the standard deviation. For calculating this mean, the signal of W = 5 mm is disregarded, since this signal is dispersed. The theoretical group velocity of tungsten, equal to 2814 m s^{-1}, lies within this range.

Table 4.3: The values of the group velocity for different width dimensions.

Width (mm)	V_{group} (m s^{-1})
5	2501
6	2826
7	2816
8	2810
9	2805
10	2801
11	2847
12	2847
13	2850
14	2853
15	2852

In table 4.3, the group velocity seems to stabilize for plate widths larger than 10 mm. The relative error of the group velocity, for a plate width of 11 mm, compared to the theoretical value, has a value of 1.2%. There could be several reasons for this error: the physics chosen for the waveguide ('shell') might not be accurate or the plate might not be long enough. The longer plate, the less the measurements are affected by the diffraction of the excited pulse. Moreover, the wider the plate compared to the transducer, the more diffraction occurs. The optimal ratio between the plate width, transducer width and plate length might be obtained from table 4.3.

In table 4.3, it can be seen that between the widths 10 mm and 11 mm , the group velocity makes a sudden change. Since the plate length is 20 mm, the plate width becomes less than half the plate length around 11 mm. Moreover, around 11 mm, the plate width is more than twice the size of the transducers size. A plate with a width less than half the size of the length and a transducer width more than half the size of the plate width, seem to be the optimal dimensions for a waveguide. However, more research should be done to verify this statement.

4.2 Time Step Size

To minimize the solving time, the optimal time step size is estimated using a model without the immersion fluid. The dimensions (LxWxD) of the plate is 20mm x 11mm x 0.1mm and the material of the plate is Tungsten. The width of 11mm is chosen as a result of the findings in the in the previous section. Here, it was found that for a plate width larger than 10 mm, the group velocity stabilized.

The transducer on top of the plate has a width of 4.8 mm and sends a 5-cycle sinus pulse into the plate with an amplitude of 0.1 m and a frequency of 2 MHz. The plate, with W = 11 mm, has therefore a frequency width product of 22 MHz·mm. For the mesh, a size of 8 mesh elements per wavelength is used.

4.2.1 Parametric Sweep

With an parametric sweep, the Courant–Friedrichs–Lewy number from equation 3.2 was varied from 0.02 to 0.2 with steps of 0.02. In the figure below, the acquired plot of the parametric sweep is shown.

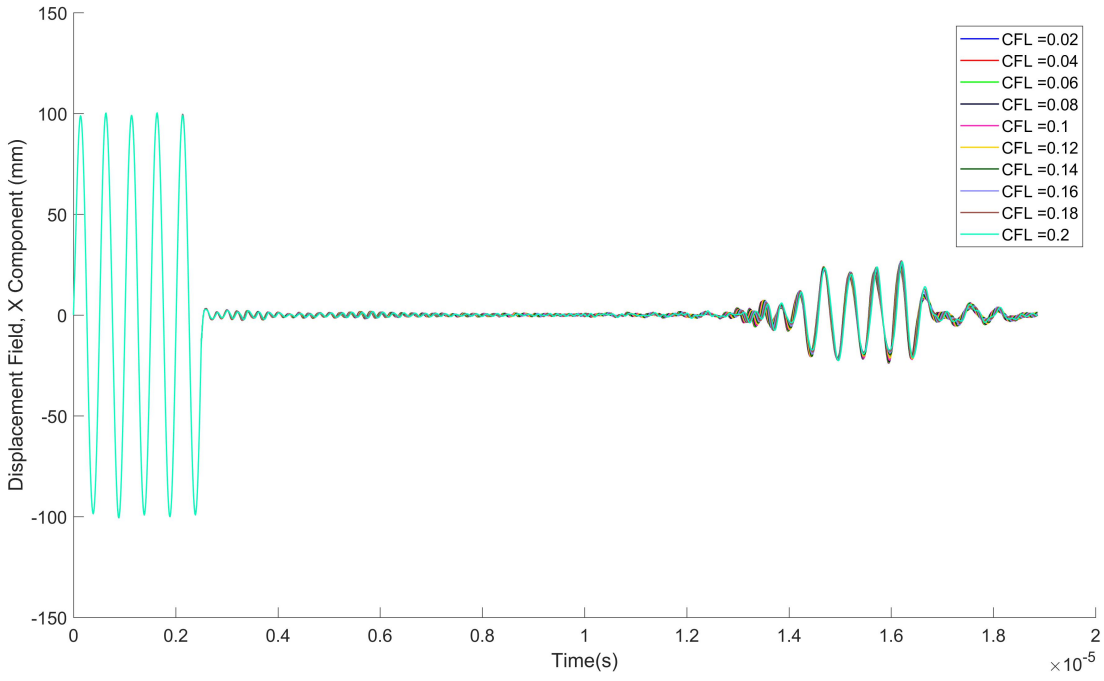

Figure 4.4: The SH0 wave measured on top of the waveguide with a boundary point probe. Displacement field in the x-direction plotted again the time.

In figure 4.4, it can be seen that the peak time's around 16.2 μs, seem to change the most for the different CFL numbers, compared to the other peaks.

In figure 4.5, the peaks around 16.2 μs can be seen.

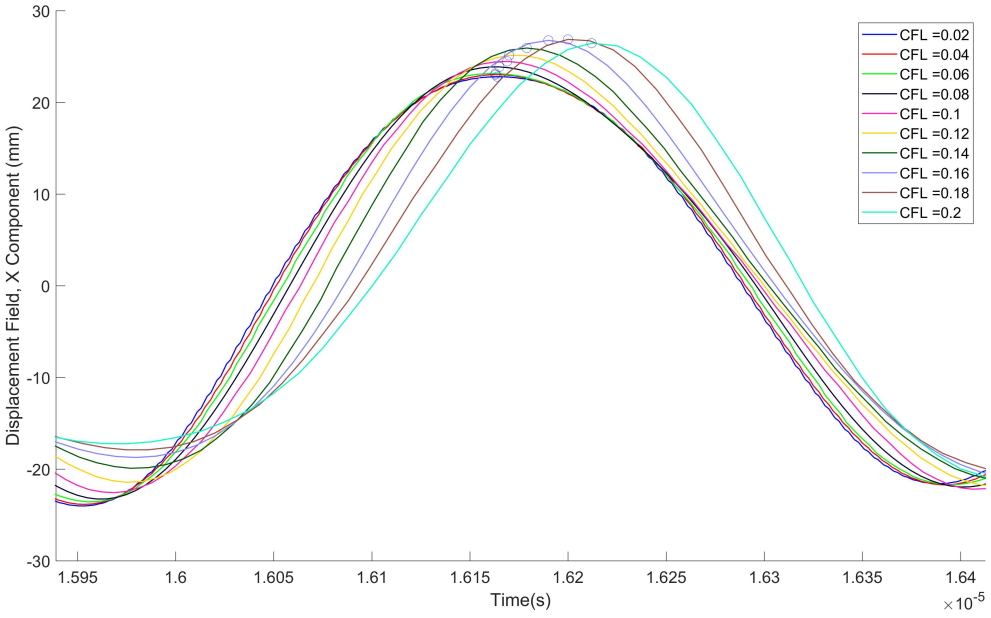

Figure 4.5: SH0 peaks of different CFL numbers .

The values of the peak time, for the different CFL number, of figure 4.5, are stated in the table 4.4.

Table 4.4: The results from the COMSOL model. The CFL numbers and the corresponding peak time's.

CFL	Peak Time (μs)
0.0200	16.1640
0.0400	16.1630
0.0600	16.1630
0.0800	16.1650
0.1000	16.1690
0.1200	16.1700
0.1400	16.1790
0.1600	16.1900
0.1800	16.2000
0.2000	16.2120

In the figure below, the values from table 4.4 are plotted.

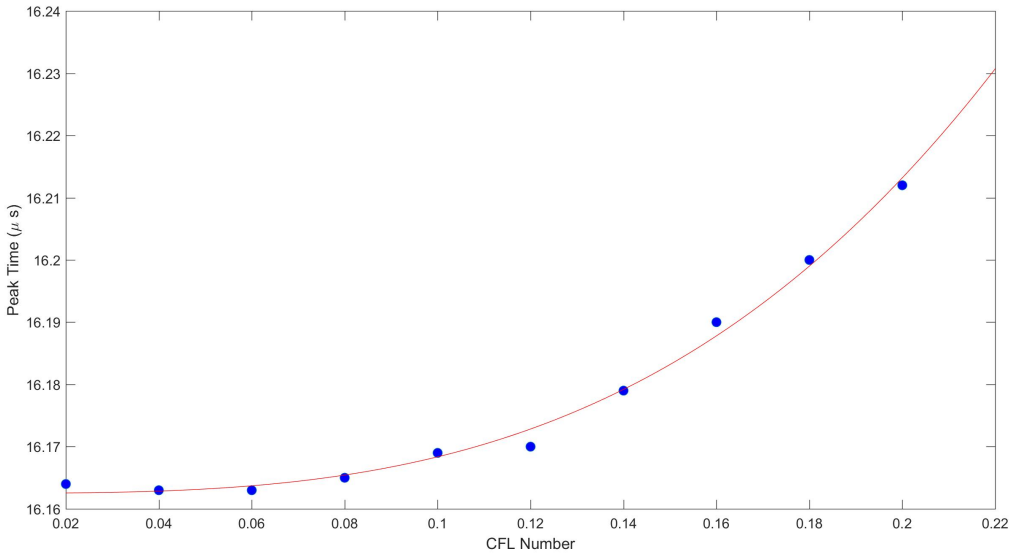

Figure 4.6: The Displacement in the x-direction plotted against the corresponding CFL numbers .

The fitted line is a power function as given in equation 4.1. Here, a = 7.643 ± 6.867, b = 3.117 ± 0.553 and c = 16.16 ± 0.01.

In figure 4.6, the values for the peak time asymptoticly approach a stable value around CFL = 0.08. Therefore, the optimal CFL number seems to be around 0.08.

4.2.2 Accuracy

With the cross correlation function, the time delay of the returning pulse was evaluated. The resulting values of the time delay, can be found in table 4.5. The mean value, of the data points given in table 4.5, was calculated to be 14.13 ± 0.13 μs, where 0.13 is the standard deviation.

Table 4.5: The values for the time delay for every CFL number.

CFL	Time Delay (μs)
0.0200	14.0425
0.0400	14.0425
0.0600	14.0437
0.0800	14.0450
0.1000	14.0500
0.1200	14.0550
0.1400	14.0613
0.1600	14.3100
0.1800	14.3212
0.2000	14.3250

For the parametric sweep of the CFL value, 10 data points were used. The mean group velocity, of these 10 data points, is calculated to be equal to 2831 ± 26 m s^{-1}, where ± 26 is the standard deviation. The theoretical group velocity of 2814 ms^{-1}, lies within this range.

Table 4.6: The values of the group velocity for different CFL numbers.

CFL	V_{group} (m s^{-1})
0.0200	2849
0.0400	2849
0.0600	2848
0.0800	2848
0.1000	2847
0.1200	2846
0.1400	2845
0.1600	2795
0.1800	2793
0.2000	2792

The mean value of 2831 ± 26 m s^{-1} deviates 1.5% from literature value of 2790 ± 33 m s^{-1} [28]. The tungsten used in this literature has mostly the same material properties as the tungsten used by the model, except for the density. The density in this literature study is 2 % higher than the density used in the model. Since the group velocity is inversely proportional to the squire root of the density, the expected group velocity should be 1.01% higher than 2790 m s^{-1}. Therefore, the mean value of the group velocity, found by the model, deviated 0.5% from the expected value of 2818 ± 33 m s^{-1}, estimated from the literature.

Chapter 5

Conclusion

The goal of this research is to optimize the setup of the ultrasonic viscometer with a finite element software. For this optimization, the initial aim was to investigate the influence of the volume of the fluid, in which the waveguide is immersed, on the attenuation.

For this research an accurate model was needed. To improve the accuracy of the model the optimal time step size of the solver was investigated by evaluating the peak time of the returning pulse for different CFL numbers.

To find a balance between accuracy of the model and computation time, the size of the plate was minimized. The accuracy of the model was studied by comparing the group velocity of the ultrasonic wave, computed by the model, to the theoretical value.

However, within the time frame of this research it was, unfortunately, not possible to investigate the influence of the volume of the fluid on the attenuation. Since prior knowledge about the finite element program COMSOL lacked, the research took longer than expected. Therefore, only the optimization of the time step size of the solver and the optimal plate width were investigated.

For a pulse frequency of 2 MHz, the smallest possible width for the tungsten plate was found to be 6 mm. Therefore, the critical frequency width product was found to have a value of 12 MHz·mm.

An interesting finding was that for the values higher than this critical frequency width product, the time delay of the returning pulse, asymptoticly approached a stable value around a plate width of 10 mm. Therefore, an optimal frequency width product was found: 20 MHz·mm. This optimal value could be related to the size of the transducer. For a pulse frequency of 2 MHz, the optimal plate width was more or less twice the size of the transducer. It should be investigated if this also applies to the real transducer size. For this, a parametric sweep could be done over different dimensions for the width of the plate, while using the real size of the transducer.

The group velocities, stabilized for plate widths larger than 10 mm. The relative error of the group velocity, found by the model, had a value of 1.2% for a plate width of 11 mm. There are two possible causes for this error: the physics in the model for the waveguide might be inaccurate or the length of the plate is too small. A longer plate will be less affected by the diffraction of the exited pulse. The wider the plate, compared to the transducer, the more diffraction occurs. There should be an optimal ratio between the plate width, transducer width and plate length. It should be investigated if the relative error becomes smaller with these optimal dimensions of the plate and transducer.

For the width study, the value of the group velocity is found to be 2830 ± 21 ms^{-1}. The theoretical value of 2814 ms^{-1} lies within this range.

The optimal CFL number was found to be 0.08. Moreover, the group velocity, for the CFL parametric sweep, was found to be equal to 2831 ± 26 ms^{-1}. The theoretical value lies within this range.

It is recommended for future studies to investigate if the attenuation is affected by the plate width.

Since the attenuation is calculated by the difference in signal strengths, between two immersion depth, the attenuation might not be affected by the inaccuracy of the model introduced by the plate width. This plate width study should be done for plate width's above the critical plate width of 6mm.

For a more accurate model, it is recommended to include the conversion of the electrical energy, of the transducer, to the kinetic energy. In this model, the sinusoidal pulse of the transducer is directly set as the displacement in the plate, without considering how much displacement a certain voltage would introduce.

Appendix A

Wave Propagation in Fluid

In fluids, waves consist of alternative compressions and refractions[13]. Newtons law of motion can therefore be expressed in pressure and displacement. The wave equation for an one-dimensional case can be written as

$$\frac{\partial p}{\partial x} = -\rho_0 \frac{\partial^2 u}{\partial^2 t}, \tag{A.1}$$

where ρ_0 is the density of the fluid.
The relation between pressure and the compression of fluids can be expressed as follows

$$p = -\frac{1}{\chi}\frac{\partial u}{\partial x}, \tag{A.2}$$

where χ is the compressibility, which is defined as follows

$$\chi = -\frac{1}{V}(\frac{\partial V}{\partial p}). \tag{A.3}$$

Combining equation A.1 and equation A.2, gives the following expression

$$\frac{\partial^2 u}{\partial^2 t} = V_0^2 \frac{\partial^2 u}{\partial^2 x}, \tag{A.4}$$

where V_0 is defined as

$$V_0^2 = \frac{1}{\chi \rho_0} = \frac{\partial p}{\rho}. \tag{A.5}$$

For a three-dimensional case, equation A.4 can be generalized into the following forms

$$\frac{1}{V_0^2}\frac{\partial^2 \vec{u}}{\partial^2 t} = \nabla^2 \vec{u}. \tag{A.6}$$

In contrary to solids, fluids and gases do not have shear waves, due to the absence of shape elasticity[11]. Therefore, the motion of wave, $\vec{u}$ can be expressed as follows

$$\vec{u} = \vec{\nabla}\varphi, \tag{A.7}$$

where φ has the following form

$$\varphi = Ce^{j(kx-\omega t)}. \tag{A.8}$$

Wave equation A.6 applies for inviscid fluids. To find the wave propagation for fluids with viscosity, the linearized Navier-Stokes equation is used[18].

$$\frac{\partial^2 \vec{u}}{\partial t^2} = -\frac{1}{\rho_0}\vec{\nabla} p + \upsilon \nabla^2 \frac{\partial \vec{u}}{\partial t} + \frac{\upsilon}{3}\vec{\nabla}(\vec{\nabla} \cdot \frac{\partial \vec{u}}{\partial t}) \tag{A.9}$$

Here, υ is the kinematic viscosity[12].
Combining equations A.2, A.4, A.7 and A.9 gives the following expression

$$\frac{\partial^2 \varphi}{\partial^2 t} - V_0^2 \nabla^2 \varphi - \frac{4\upsilon}{3}\nabla^2 \frac{\partial \varphi}{\partial t} = 0. \tag{A.10}$$

Combining A.8 and A.10 the following dispersion relation can be found

$$\omega^2 - V_0^2 k^2 + j\frac{4\upsilon}{3}\omega k^2 = 0, \tag{A.11}$$

which can be solved for k.

$$\begin{aligned} k^2 &= \frac{\omega^2}{V_0^2 - j\frac{4\upsilon}{3}\omega}, \\ \Rightarrow k &\approx \pm\frac{\omega}{V_0}\left[1 + j\frac{2\upsilon\omega}{3V_0^2}\right] \end{aligned} \tag{A.12}$$

The imaginary part of equation A.12 is the absorption of acoustic wave energy by the medium, also known as attenuation[13]. Since there are no shear waves in the fluid, this attenuation applies for longitudinal waves.

Appendix B

Solid-Fluid Interface

Incident plane waves from a solid at the interface of a fluid will be partial reflected and partial transmitted into the other media. The effects of a solid-fluid interface on a wave, can be described by the reflection and transmission coefficient.

In figure B.1, the phase shift due to reflection and transmission at the fluid-solid interface can be seen. The reflection and transmission coefficient from a fluid-solid interface will be the same for a solid-fluid interface[13].

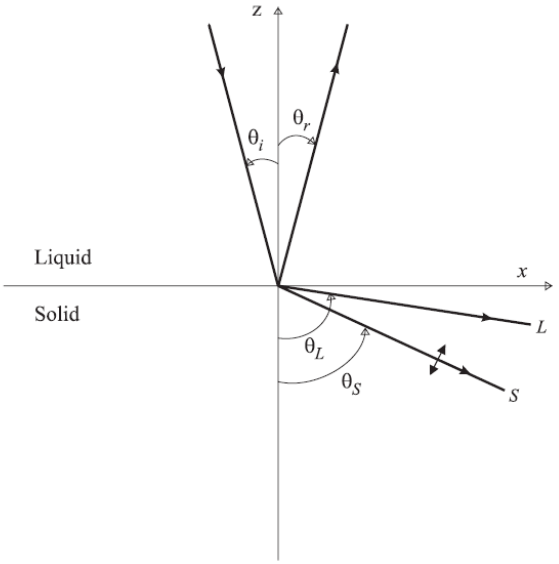

Figure B.1: Reflection and transmission at a fluid-solid interface[13].

As discussed, the displacement of waves in fluids and solids, in vectorial form, are expressed as

$$\begin{aligned} \vec{u} &= \vec{\nabla}\phi + \vec{\nabla} \times \vec{\psi}, \\ \vec{u} &= \vec{\nabla}\varphi. \end{aligned} \tag{B.1}$$

The plane wave solutions for the fluid-solid interface have the following form

$$\begin{aligned} \varphi_i &= expj\left(\omega t - k_F sin\theta_i x + k_F cos\theta_i z\right), \\ \varphi_r &= Rexpj\left(\omega t - k_F sin\theta_r x - k_F cos\theta_r z\right), \\ \phi &= T_L expj\left(\omega t - k_L sin\theta_L x + k_L cos\theta_L z\right), \\ \psi &= T_S expj\left(\omega t - k_S sin\theta_{lS} x + k_S cos\theta_S z\right). \end{aligned} \tag{B.2}$$

where k_F is the longitudinal wavenumber in a fluid, k_L the longitudinal wavenumber in a solid, k_S the shear wavenumber in a solid, R the reflection coefficient, T_L the longitudinal transmission coefficient and T_S the shear transmission coefficient.

There are three important boundaries to consider for a fluid-solid interface. These boundaries include: the continuity of normal velocities, the continuation of normal stress and the zero tangential stress in fluids[13].

The boundary condition for the continuity of normal velocities can be expressed as follows

$$\frac{\partial \varphi}{\partial z} = \frac{\partial \phi}{\partial z} + \frac{\partial \psi}{\partial x}. \tag{B.3}$$

The boundary conditions for the continuation of normal stress are given by

$$\begin{aligned} p &= \sigma_{xx}, \\ \Rightarrow V_0^2 \rho_0 \nabla^2 \varphi &= \lambda \nabla^2 \phi + 2\mu \left(\frac{\partial^2 \phi}{\partial z^2} + \frac{\partial^2 \phi}{\partial x \partial z} \right). \end{aligned} \tag{B.4}$$

The zero tangential stress in fluids results into the following boundary conditions

$$\begin{aligned} \sigma_{xz} &= 0, \\ \frac{\partial^2 \psi}{\partial x^2} + 2\frac{\partial^2 \phi}{\partial x \partial z} - \frac{\partial^2 \psi}{\partial z^2} &= 0. \end{aligned} \tag{B.5}$$

From these boundary conditions, Snell's law can be obtained.

$$\frac{sin\theta_i}{V_0} = \frac{sin\theta_r}{V_0} = \frac{sin\theta_L}{V_L} = \frac{sin\theta_S}{V_S} \tag{B.6}$$

Here, θ_r is the angle of incidence, θ_i the angle of reflection, θ_L the angle of transmission for the longitudinal waves and θ_s the angle of transmission for shear waves. Here, θ_i is equal to θ_r.

The following three equations can be obtained from the boundary conditions

$$\begin{aligned} k_F cos\theta_i R + k_L cos\theta_L T_L - k_S sin\theta_S T_S &= k_F cos\theta_i, \\ k_L^2 sin2\theta_L T_L + k_S^2 cos2\theta_S T_S &= 0, \\ \rho_0 R + \rho \left[2\frac{k_L^2}{k_S^2} sin^2\theta_L - 1 \right] T_L - \rho sin2\theta_S T_S &= 0. \end{aligned} \tag{B.7}$$

The solution of these equations are as follows

$$\begin{aligned} R &= \frac{Z_L cos^2 2\theta_S + Z_S sin^2 2\theta_S - Z_1}{Z_L cos^2 2\theta_2 + Z_S sin^2 2\theta_S + Z_1}, \\ T_L &= \left(\frac{\rho_1}{\rho_2}\right) \frac{2Z_L cos2\theta_S}{Z_L cos^2 2\theta_2 + Z_S sin^2 2\theta_S + Z_1}, \\ T_S &= -\left(\frac{\rho_1}{\rho_2}\right) \frac{2Z_S cos2\theta_S}{Z_L cos^2 2\theta_2 + Z_S sin^2 2\theta_S + Z_1}, \end{aligned} \tag{B.8}$$

where Z_1, Z_L and Z_S are defined as follows

$$\begin{aligned} Z_1 &= \frac{\rho_1 V_1}{cos\theta_i}, \\ Z_L &= \frac{\rho_2 V_L}{cos\theta_L}, \\ Z_S &= \frac{\rho_2 V_S}{cos\theta_S}. \end{aligned} \tag{B.9}$$

Appendix C

COMSOL Parameters

In the following table, the parameters used in the COMSOL model are shown. The expressions showed in the table do not apply for every study. In cases of parametric sweep, the parameters are stated in the results and discussion under the corresponding subsection.

Table C.1: The parameters used in the COMSOL model.

Parameter	Expression	Description
f0	2[MHz]	Signal frequency
T0	1/f0	Period of signal
V_SH	2810 [m/s]	Estimated shear velocity
t_pulse	N_sin/f0	Pulse duration
t_end	L/V_SH*2.5	End time for study
t_step	a/(f0*N)	Time step
N	8	Number of mesh elements per wavelength
a	0.01	CFL number
mesh	V_SH/f0/N	Mesh size
L	20[mm]	Length plate
D	0.1[mm]	Thickness plate
W	11[mm]	Width plate
L_w	10[mm]	Length water vessel
W_w	12[mm]	Width water vessel
D_w	2[mm]	Thickness water vessel
Dis	8.5[mm]	Immersion depth plate
N_sin	5	Number of cycles of the sin pulse

Bibliography

[1] SAMOFAR. Project. `http://samofar.eu/project/`. Online; accessed 9-11-2018.

[2] Jérôme Serp, Michel Allibert, Ondřej Beneš, Sylvie Delpech, Olga Feynberg, Véronique Ghetta, Daniel Heuer, David Holcomb, Victor Ignatiev, Jan Leen Kloosterman, Lelio Luzzi, Elsa Merle-Lucotte, Jan Uhlíř, Ritsuo Yoshioka, and Dai Zhimin. The molten salt reactor (msr) in generation iv: Overview and perspectives. *Progress in Nuclear Energy*, 77:308 – 319, 2014.

[3] M. Allibert, M. Aufiero, M. Brovchenko, S. Delpech, V. Ghetta, D. Heuer, A. Laureau, and E. Merle-Lucotte. 7 - molten salt fast reactors. In Igor L. Pioro, editor, *Handbook of Generation IV Nuclear Reactors*, Woodhead Publishing Series in Energy, pages 157 – 188. Woodhead Publishing, 2016.

[4] Manuele Aufiero, Mariya Brovchenko, Antonio Cammi, Ivor Clifford, Olivier Geoffroy, Daniel Heuer, Axel Laureau, Mario Losa, Lelio Luzzi, Elsa Merle-Lucotte, Marco E. Ricotti, and Hervé Rouch. Calculating the effective delayed neutron fraction in the molten salt fast reactor: Analytical, deterministic and monte carlo approaches. *Annals of Nuclear Energy*, 65:78 – 90, 2014.

[5] Sara Mastromarino. Determination of thermodynamic properties of molten salts. Periodic report, Delft University of Technology, the Netherlands, 2017.

[6] Marc van den Berg. Viscosity determination using the quasi-Scholte wave. Master's thesis, Delft University of Technology, the Netherlands, 2018.

[7] Peter Cawley and Frederick Bert Cegla. Ultrasonic nondestructive testing., 2016.

[8] Jiuhong Jia, Qiyue Wang, Zuoyu Liao, Yun Tu, and Shan-Tung Tu. Design of waveguide bars for transmitting a pure shear horizontal wave to monitor high temperature components. *Materials*, 10(9):1027, 2017.

[9] H.A.J. Froeling. Causes of spurious echoes by ultrasonic wave simulation. Bachelor's thesis, Delft University of Technology, the Netherlands, 2017.

[10] Warren C Young and Richard Budynas. *Roark's Formulas for Stress and Strain (7th Edition)*. McGraw-Hill Professional Publishing, 2001.

[11] Z. T. Nazarchuk, Valentyn Skalskyi, and Oleh Serhiyenko. *Acoustic emission: methodology and application*, pages 29–36. Springer, 2017.

[12] Jan D. Achenbach. *Wave propagation in elastic solids*. NH, Elsevier, 1999.

[13] J. David N. Cheeke. *Fundamentals and applications of ultrasonic waves*. CRC Press Taylor and Francis Group, 2017.

[14] Carlos Felippa. *Stress-Strain Material Laws*. University of Colorado, 2016.

[15] Omar Falou. Modelling high frequency ultrasound scattering from cells and ultrasound contrast agents. 2018.

[16] Wiesław Ostachowicz. *Guided waves in structures for SHM: the time-domain spectral element method*. Wiley, 2012.

[17] Karl F. Graff. *Wave motion in elastic solids*. Dover Publications, 1991.

[18] Peter Hagedorn and Anirvan DasGupta. *Vibrations and waves in continuous mechanical systems*. Wiley, 2007.

[19] F B Cegla, P Cawley, and M J S Lowe. Fluid bulk velocity and attenuation measurements in non-newtonian liquids using a dipstick sensor. *Measurement Science and Technology*, 17(2):264–274, 2005.

[20] COMSOL Multiphysics. *version 5.2a*. COMSOL Inc., Zoetermeer, the Netherlands, 20178.

[21] Kim B. Shedd. Metal prices in the united states through 2010: U.s. geological survey scientific investigations report. *U.S. Geological Survey*, (5188):187, 2013.

[22] Mads Herring Jensen. Theory of thermoviscous acoustics: Thermal and viscous losses. `https://www.comsol.com/blogs/theory-of-thermoviscous-acoustics-thermal-and-viscous-losses/`, 2014. Online; accessed 9-11-2018.

[23] Ashish Kumar Singh. Coupling structural mechanics interfaces. `https://www.comsol.com/blogs/coupling-structural-mechanics-interfaces/`, 2014. Online; accessed 9-11-2018.

[24] A.R. de Reuver. Temperature dependence of the attenuation and group velocity of ultrasonic waves in tungsten. Bachelor's thesis, Delft University of Technology, the Netherlands, 2018.

[25] Guilherme Caminha. The cfl condition and how to choose your timestep size. `https://www.simscale.com/blog/2017/08/cfl-condition/`, 2018. Online; accessed 24-09-2018.

[26] Comsol Support. Resolving time-dependent waves. `https://www.comsol.com/support/knowledgebase/1118/`, 2018. Online; accessed 24-09-2018.

[27] MATLAB. *version R2017a*. The MathWorks Inc., Eindhoven, the Netherlands, 2017.

[28] H T Lee, S Ando, J W Coenen, Y Mao, J Riesch, H Gietl, R Kasada, Y Hamaji, K Ibano, and Y Ueda. Longitudinal and shear wave velocities in pure tungsten and tungsten fiber-reinforced tungsten composites. *Physica Scripta*, 2017(T170):014024, 2017.